ARTICLE

Photoelectrochemical water splitting by triazine based covalent organic framework

Anirban Pradhan,*[a] and Matthew A. Addicoat[b]

Received 00th January 20xx,
Accepted 00th January 20xx

DOI: 10.1039/x0xx00000x

Photo electrochemical (PEC) water splitting under visible light irradiation is a very promising path for green and sustainable hydrogen production. PEC process has gained attracted enormous research interest due to the potential of direct conversion of solar power into chemical fuel. Herein, we present a covalent organic framework (COF) which shows promise as an ideal photoabsorber due to the combination of efficient light harvesting sites with a suitable band gap and catalytic sites for HER. Under solvothermal condition a Schiff base type condensation between 1,3,5-tris (4-formylbiphenyl) benzene (TFBB), 2, 4, 6-Tris(4-aminophenyl)-1, 3, 5-triazine (TAT) and 2, 4, 6-Tris(4-aminophenyl)-benzene (TAB) yields a crystalline, 2-D covalent organic frameworks TFBB-TAT and TFBB-TAB COF respectively. The as prepared triazine containing TFBB-TAT COF shows better photo electrochemical (PEC) water splitting compared to non-triazine based TFBB-TAB COF. This work enriches the structural variety of COFs and plays an important role in PEC water splitting, also illustrating the intriguing electrochemical behaviour of this class of materials.

Introduction:

The progressive decrease of fossil fuel reserves gives rise to an acute urgency for clean, sustainable and environmentally viable energy sources.[1,2] Till now, solar energy is the major sustainable energy source in the global energy supply. During the last decades, several research groups around the world have continuously tried to develop and improve a visible light photocatalytic system as a green technology which is capable of direct conversion of solar energy into chemical energy, stored in the bonds of "solar fuels" or "chemical fuels" such as hydrogen.[3-5] However, the biggest challenges for large scale utilization of these green technologies are minimizing the hydrogen production cost whilst maximising the efficiency at a lower economic investment. This problem can be solved by using photo electrochemical (PEC) water splitting cells which directly split water in presence of sunlight to hydrogen and oxygen at cathode and anode respectively.[6-8] Thus development of an efficient photocatalytic system became an active field of energy research to design efficient photoelectrodes. For this purpose, the physicochemical properties of PEC catalysts such as suitable band gap, favourable band edge positions, surface area, morphology, interfacial charge transfer kinetics and corrosion stability all play an important role.[9-11] Various inorganic and organic photocatalysts have been developed but compared to inorganic semiconductors, organic semiconductors such as graphitic carbon nitride (g-C_3N_4) tend to perform less efficiently. Despite this, g-C_3N_4 and many derivatives thereof have been widely exploited due to their tailored structure, excellent electronic properties and diverse synthetic modularity.[12-16]

Covalent organic frameworks (COFs) are a class of crystalline porous material in which organic monomers integrate to form a periodic framework.[17-20] In the last few years COFs have been suggested and developed as new photoactive materials for light-induced hydrogen evolution because of the high electron density that comes with an extended π-stacked structure similar to g-C_3N_4 as well as distinct porosity.[21] Furthermore, the photochemical activity can be precisely tailored by the selection of proper building unit. COFs are modular, versatile, and adaptive as they are characterized by an easy tunability of (opto) electronic properties, structure, crystallinity, and porosity. They are mainly composed of highly abundant organic elements (C, H, N, O, S *etc.*) which allows synthetic versatility. The extended in plane π-electron conjugation together with the possibility of axial charge transport in the stacking direction by the overlap of π-orbitals can result in high charge carrier mobility.[22-23] Such characteristics of supramolecular COF architectures promote light harvesting and charge transport capacity.

Photoelectrochemical water splitting is mainly determined by two key factors. One is the suitable valance and conduction band position in which the electrons are exited from valence band by photon irradiation. Mostly, the photoactive characteristics of nitrogen-rich COFs are determined by the nitrogen group present in the COF system. In this context the triazine moiety was found to be a promising photoabsorber site in various polymer or COF systems. The band position of triazine containing photocatalysts is mostly influenced by the N_{2p} orbitals of the triazine moiety. The second PEC governing factor is the electrocatalytic activation of proton by charge recombination to generate molecular hydrogen. Up to now, modified g-C_3N_4 and its derivatives were used as a stable photocatalyst for proton reduction under visible light irradiation. However, their improper band alignment retards the

[a] Department of Chemistry, Birla Institute of Technology (BIT) – Mesra, Ranchi, Jharkhand, 835215, India. Email: anirbanpradhan@bitmesra.ac.in
[b] School of Science and Technology, Nottingham Trent University, Clifton Lane, Nottingham, NG11 8NS, UK.

† Footnotes relating to the title and/or authors should appear here.
Electronic Supplementary Information (ESI) available: [details of any supplementary information available should be included here]. See DOI: 10.1039/x0xx00000x

efficiency of proton reduction. Recently, Jijia *et al* reported a covalent triazine polymer/COF by

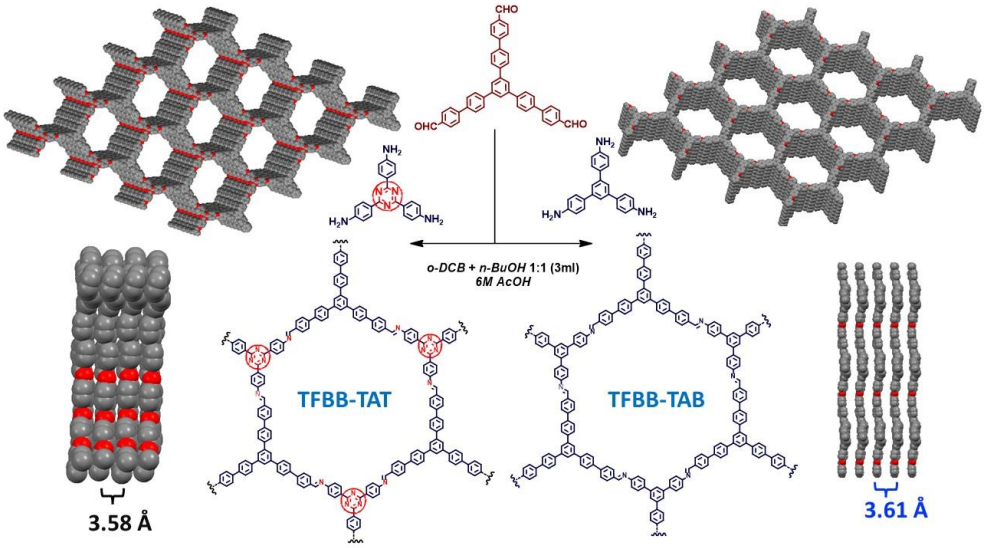

Scheme 1: Schematic presentation of TFBB-TAT and TFBB-TAB COF

changing the C and N ratio, making the band alignment suitable for proton reduction as well as water oxidation.[24] Very few imine and hydrazine based COFs have been explored for photo electrochemical (PEC) water splitting under visible light irradiation.[25] There are some

significant drawbacks for employing COF materials: their instability and poor energy conversion in neutral water. In our previous study, we reported porphyrin based metal free COP/COF for electrochemical water splitting in acidic medium.[26-28] In the last few years Lotsch *et al* have explored covalent triazine-based COF materials as photocatalysts with high thermal and chemical stability.[29-30] The extended π-staking in triazine based COFs promotes exciton separation and excellent charge transport properties which is required for photocatalysis.[31,] So far, these COFs have been explored as potential sorbents and as catalytic support.[32] Exploration of related structures and comparison with triazine-based COFs with COFs of similar structure but lacking the central triazine unit has not yet been directly explored for photocatalysis. Based upon the superior performance of the triazine containing Covalent Triazine Framework (CTF), herein we introduce a triazine based covalent organic framework (TFBB-TAT) which shows favourable water splitting compared with the triazine-free counterpart TFBB-TAB COF (**Scheme 1**). The diversity and easily tailored structures for tunable water splitting capacity may not only widen the scope of organic semiconductors but also provide a molecular level understanding and comparison of the inherent heterogeneous photocatalysis.

Result and Discussion:

The crystallinity of both TFBB-TAT and TFBB-TAB COFs were assessed by powder x-ray diffraction (PXRD) analysis (**figure 1**a & **c**). An intense peak at 2θ value of 3.27° and 3.16° observed for TFBB-TAT and TFBB-TAB COF, indicates the first (100) plane. Other minor peaks ~ 5.4° and 6.2° indicate the presence of (200) planes. The broad peak for TFBB-TAT COF observed at ~25° (2θ) stipulates the (001) facets usually observed for amorphous polymers, which indicates the presence of strong interlayer π−π stacking also suggests the periodicity of the 2D COFs is extended to the third dimension.[33] This large stacking is due to the planar triazine unit (coming from TAT) in the COF crystallites, which is absent for the TFBB-TAB COF. Due to the presence of the non-planar central phenyl ring (coming from TAB), interlayer stacking for TFBB-TAB COF is very poor. The Stacking distance between the two adjacent layers for TFBB-TAT and TFBB-TAB COF are 3.58 and 3.61 Å respectively. Pawley refinement based on Density Functional based Tight Binding (DFTB) calculated structures, was carried out to determine the exact lattice packing for both of these COFs. TFBB-TAT shows slipped-AA stacking with a stacking energy -~~28~~36.~~3~~27 kcal mol^{-1} and TFBB-TAB COF also shows slip-AA stacking with -~~27~~8.98~~84.62~~ kcal mol^{-1} stabilization energy per unit cell. The calculated and experimental PXRD patterns match well with this stacking mode. After refinement, the unit cell parameter was calculated to be a = 33.25 Å, b = 34.26, c = 7.22 Å, α = β = 90°, γ = 59° (R_{wp} = 2.59%, R_p = 2.11%) for TFBB-TAT COF and a = 33.04 Å, b = 34.18, c = 7.16 Å, α =89°, β = 88°, γ = 59° (R_{wp} = 3.40%, R_p = 2.41%) for TFBB-TAB COF (**Figure 1b & d**).[34] Stabilization of this slipped-AA stacking over the eclipsed (AA) stacking is due to less repulsion between the atoms where the atom lies slightly offset to the adjacent layers. To confirm the permanent porosity of these two COFs (TFBB-TAT and TFBB-TAB), N_2 adsorption-desorption measurement were carried out. A typical type IV adsorption

isotherm was observed along with a sharp capillary condensation, indicating the presence of mesopores in TFBB-TAT and TFBB-TAB COF (Figure 2a&b) structures.[35] and a surface area of 729 m^2 g^{-1}, pore width = 3.48 nm and 130 m^2 g^{-1} pore

is absent in the TFBB-TAB COF (**Figure 2k**). Fourier transform infrared spectroscopy (FT-IR) reveals the presence of the aldehyde -C-H stretching band of TFBB at 2730 cm^{-1} which is impaired after the condensation reaction to form TFBB-TAT

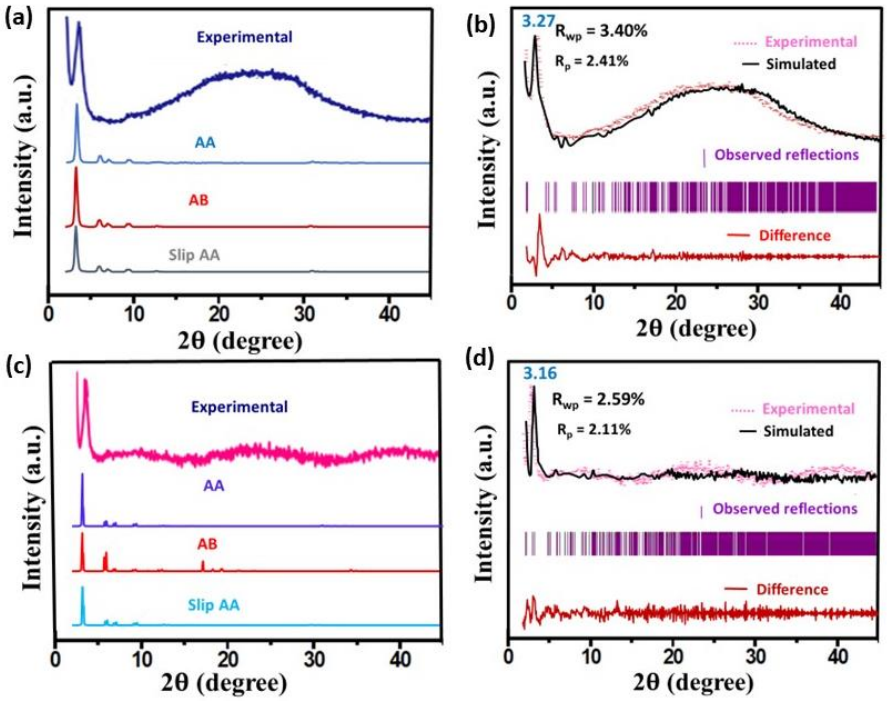

Figure 1: (a, c) Experimental and theoretical powder x-ray diffraction comparison of TFBB-TAT and TFBB-TAB COF respectively. (b, d) Pawley refinement of the experimental PXRD of TFBB-TAT and TFBB-TAB COF respectively.

width = 3.45 nm for TFBB-TAT(figure 2a) and TFBB-TAB COF (figure 2b) respectively. The surface area were calculated by taking the value of relative pressure (P/P0) from 0.07 to 0.2 with a total pore volume of 0.244 cc g-1 and 0.05 cc g-1 for TFBB-TAT and TFBB-TAB respectively at P/P0 = 0.99. A high surface area for TFBB-TAT was measured, due to the strong stacking throughout long channels of COF crystallite. It is reported that the central triazine moiety is more planar than the central phenyl ring with respect to the other phenyl ring in both the COFs.

This makes the TFBB-TAT COF more planar, and increases the interlayer stacking. H1 type hysteresis observed (**Figure 2a&b**) in both COFs isotherm with a gradual increase in N_2 uptake at higher pressure, indicating towards mesopores generated *via* the aggregation of spherical particles.[36] Different carbon environment was confirmed by the solid state ^{13}C cross polarisation magic anglespinning (CP-MAS) NMR spectroscopy. Characteristic imine bonded carbon (-C=N-) was reaffirmed by the chemical shift of ~164 ppm for TFBB-TAT and ~162 ppm for TFBB-TAB. One extra deshielded peak at 173 ppm, was confirmed as the presence of triazine carbon atom of TFBB-TAT COF, which

and TFBB-TAB COF (**Figure 2l**). This indicates full depletion of the starting aldehyde. Total consumption of starting amine is also confirmed by the attenuation of the –N-H stretch at 3470 cm^{-1} (TAT) and 3433 cm^{-1} (TAB) in both of the COF TFBB-TAT and TFBB-TAB respectively. Imine bond (-C=N-) formation was further confirmed by the appearance of a new peak at 1697 cm^{-1} for both the COFs, which was absent in all the precursors (TFBB, TAT, TAB). Morphological studies were investigated by the transmission electron microscopy (TEM) and scanning electron microscopy (SEM) (**Figure 2 c-j**). From the HR-TEM images, it is evident that both COFs form the hollow tubular morphology with thickness of ~400 nm, having internal diameter of ~200 nm. SEM images also support the same morphology shown by the TEM analysis. Presence of elemental carbon and nitrogen was confirmed by the X-ray photoelectron spectroscopy (XPS). The high resolution XPS analysis shows the presence of two types C_{1s} peak at ~284.0 eV, ~288.0 eV and ~283.7 eV, ~287 eV for TFBB-TAB and TFBB-TAT respectively (**Figure S4a**, **Figure S5a**). This is due the presence of -C=C and -C=N carbon atoms in the TFBB-TAT and TFBB-TAB COF moieties. Furthermore, the N 1s XPS peak

at ~398.5 eV for TFBB-TAB and ~397.5, ~400.7 eV for TFBB- TAT indicates the presence of -C=N functionality for both COF materials. Additional peak arises in TFBB- TAT COF due to presence of the triazine moiety (**Figure S4b**, **Figure S5b**). The chemical stability of the TFBB-TAT and TFBB-TAB COF have been verified by stirring the

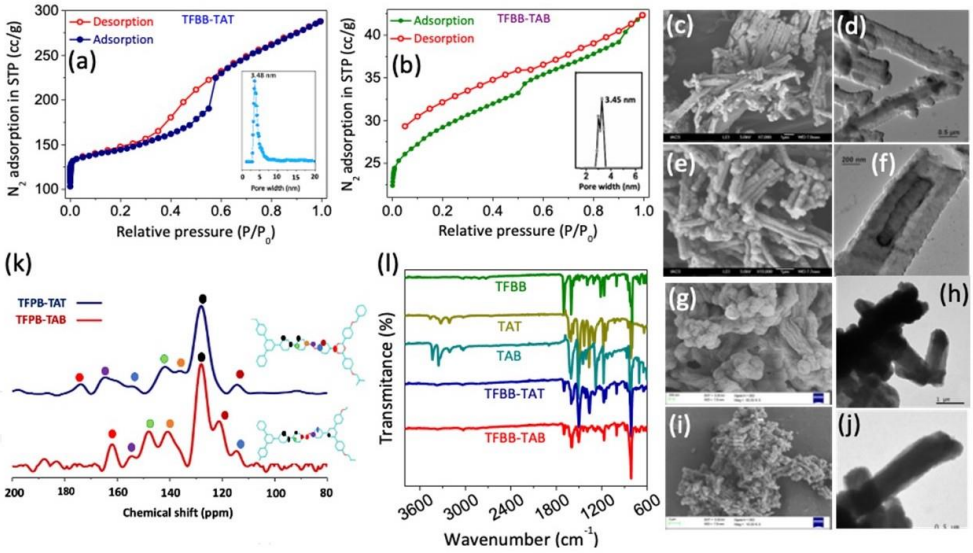

Figure 2: (a) N_2 adsorption/desorption isotherm of TFBB-TAT and TFBB-TAB COF respectively. (c, e) SEM images of TFBB-TAT COF. (d, f) HR-TEM images of TFBB-TAT COF. (g, i) SEM images of TFBB-TAB COF. (h, j) HR-TEM images of TFBB-TAT COF (k) ss13C MAS NMR spectra of TFBB-TAT and TFBB-TAB COF. (l) FT-IR spectra of TFBB-TAT and TFBB-TAB COF.

material in 2M NaOH and 2M H_2SO_4 solutions for 5 days, respectively. As shown in **Figure S6a & S6b** ESI, both the COF materials are relatively stable in 2M NaOH and 2M H_2SO_4 solutions for 5 days. This results suggested high stability and robust organic framework of TFBB-TAT and TFBB-TAB COF.[37] TFBB-TAT COF shows "Acid Responsive COFs" at low pH (1 to 3) behaviour **(ESI, Figure S7)** was protonated range and shows colour change which is absence in the case of TFBB-TAB COF. The crystallinity of the TFBB-TAT COF loses between pH 1 to 3 in solid sample but at pH 4 again we recovered original PXRD pattern **(ESI, Figure S8)**.[38] We performed post synthetic modification of imine to amine of TFBB-TAT COF material (detail procedure mentioned in supporting information, **ESI, Figure S8 & S9)**[39] FT-IR spectra revealed that after modification a new vibration band appeared at 3300-3400 cm^{-1} which was attributed to a secondary amine (ν_{N-H}) stretching mode. The intensity of the imine vibration ($\nu_{C=N}$) at 1697 cm^{-1} gradually disappeared over prolonged reaction time at 120 °C (**ESI, Figure S9**). Which agreed with previously reported procedure.[39]

PHOTOELECTROCHEMICAL ACTIVITY:

The synthesized COFs were employed as photoelectrocatalysts for water to hydrogen production in PEC. The photocathodes were designed by employing the COF material on the poly(3,4-ethylenedioxythiophene) polystyrene sulfonate (PEDOT:PSS) modified ITO surface. The PEDOT:PSS layer on ITO substrate serves as a hole transporting candidate in the photocathode. Further, the COF layer on the photocathode was in direct contact with the aqueous electrolyte. The cathodic water reduction capacity of the as synthesized COFs in PEC was studied from the polarization plots under dark and illuminated conditions. Figure 3a shows cathodic polarization plots of as synthesized COFs modified photocathodes under dark and illuminated conditions. A notable increment of cathodic current density was noticed on switching from the dark to illuminated condition. This enhancement of cathodic response attributed to the photoreactivity of the as synthesized COFs. The improved negative current density upon illumination originates from the electron-hole pair generation on the COF surface followed by transfer of the hole to PEDOT: PSS/ITO and the electron moves to the electrolyte leading to the water reduction.[40] The water reduction efficacy of a photocathode is generally determined from the magnitude of current density at 0 V vs. RHE, which signifies thermodynamic bias free condition. In the present study, the TFBB-TAT containing photocathode delivers a current density of 4.32 mA cm^{-2} which found to be much superior to the TFBB-TAB based counterpart. The higher cathodic current density achieved with TFBB-TAT photocathode reflects its potential for water reduction under visible light illumination. Moreover, the cathodic current response of the TFBB-TAT electrode was found to be superior to TFBB-TAB throughout the studied cathodic potential region. The reversibility of the photoreactivity of the synthesized COF was studied from the transient photocurrent response over several light on-off cycles. The transient photocurrent was recorded at a fixed potential of -

0.5 V vs SCE. Figure 3b represents the transient photoresponse of the designed photocathodes. A sharp increase of negative current density was noticed on light illumination whereas the current response reverts back to the initial value as the illumination is shut down. This rapid change of response current under dark and illumination state signifies good photoreversibility of the developed photocathodes. Moreover, the magnitude of transient photoresponse was found to be higher for TFBB-TAT as compared to the TFBB-TAB. Similar characteristics were noticed for the polarization which again reflects the better photoreactivity of TFBB-TAT over TFBB-TAB. The better photoreactivity of TFBB-TAT COF arises from its low band gap as compared to the TFBB-TAB counterpart and more importantly, the presence of triazine functionalities helps to improve the photoabsorption capacity in TFBB-TAT.[41] However; the TFBB-TAB counterpart does not have any such functionality for light harvesting. Thus, the photocurrent recorded in the TFBB-TAT electrode found to be enhanced compared to the TFBB-TAB counterpart. The current response recorded with present photocathodes was found to be comparable to many recently reported photocathodes.[42-44]

region. The diameter of the semicircle arc generally used to evaluate the charge transfer resistance (R_{ct}) of an electrode/electrolyte interface. A smaller diameter signifies lower charge transfer resistance and vice versa. Further, the low charge transfer resistance ascertains good charge transport from electrode to electrolyte which leads to a higher redox kinetics at the electrode surface. In present study the TFBB-TAT electrode exhibits lower Rct (17.12 Ω) than TFBB-TAB (21.74 Ω) electrode. Though, charge transfer resistance is not only the parameter for the higher proton reduction rate of TFBB-TAT COF. The high surface area of TFBB-TAT COF(729 $m^2 g^{-1}$) compare to TFBB-TAB COF (130 $m^2 g^{-1}$) offer a large electrode–electrolyte interfacial area, which results in a promising proton reduction capacity.[45] This corroborates the higher charge transfer across TFBB-TAT/electrolyte interface as compared to the TFBB-TAB/electrolyte interface which results in faster water reduction kinetics at the former electrode. Thus, the high photoresponse obtained with TFBB-TAT electrode can be attributed to its good photoabsorption capacity

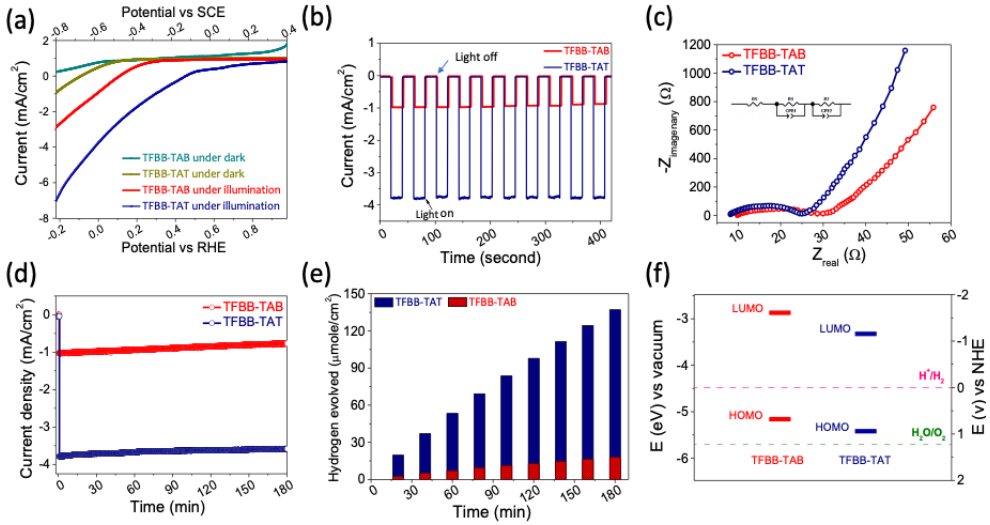

Figure 3: Photoelectrocatalytic HER activity of the TABB-TAT and TFBB-TAB COF. (a) Polarization plots of developed photocathodes under dark and illumination, (b) transient photo current response under dark and light (c) Nyquist plots of the TABB-TAT and TFBB-TAB COF (inset shows equivalent cuicuit diagram) (d) long term photostability of COF based photocathodes, (e) PEC hydrogen production profile of developed photocathodes, (f) band edge position of the developed TABB-TAT and TFBB-TAB COF.

The efficiency of a photocathode for water reduction largely depends on its charge transfer characteristics at electrode/electrolyte interface. In order to study the charge transfer process at electrode/electrolyte interface we have executed impedance measurements. The complex impedance plot, known as Nyquist plot is mostly used to understand the charge transport characteristics of an electrode/electrolyte interface. Figure 3c shows the Nyquist plots of the designed photocathodes. The Nyquist plots shows semicircle arc in 5-25 Z (Ω) region and straight line evolved in high frequency together with efficient charge transport characteristics. The potentials for HER of TFBB-TAT and TFBB-TAB COF are linearly increased with the increase of pH (**ESI, Figure S10**) value with a slope of 57 mV (ln10 × RT/F) at 25°C (details description in supporting information section).[46-47] The long term photostability of the designed photocathodes was investigated by amperometric studies under illuminated condition. The designed photocathode shows considerable retention of photocurrent density after 180 minutes of operation under visible light illumination (**figure 3d**). However, the TFBB-TAT photocathode (94% retention) exhibits better stability

than the TFBB-TAB photocathode (73% retention). The high stability of TFBB-TAT photocathode under illumination condition makes it a potential candidate for efficient PEC water splitting application. The PEC water reduction capacity of the hydrogen evolved during chronoamperometric study at -0.5 V vs. SCE. Figure 3e shows the PEC hydrogen production profile of TFBB-TAT and TFBB-TAB based photocathodes. The TFBB-TAT developed photocathode was checked by measuring the quantity of photocathode offers a hydrogen production capacity of 137 µmol cm^{-2} after 180 minutes of PEC operation. Moreover, the hydrogen production capacity of TFBB-TAT electrode is shown to be 7.6 times higher than that of the TFBB-TAB electrode. This superior hydrogen production activity of TFBB-TAT photocathode was attributed to its low band gap, higher photoabsorption capacity, and efficient charge transport capacity as compared to the TFBB-TAB photocathode. Further, the high surface area of the TFBB-TAT COF offers a large number of active sites for water reduction on electrode surface. Previous reports on nitrogen rich COFs for electrochemical water splitting (proton reduction) reveals that –C=N- functionalities serve as active centres for proton reduction by molecular hydrogen generation.[30] In present study both the synthesized COFs have –C=N- functionalities on their structural unit which can serve as the active centre for water reduction. Thus, the number of –C=N- functionalities will determine the water reduction capacity of the COF-modified photocathodes. In case of TFBB-TAT COF the number of –C=N- groups (six/structural unit) found to be two times higher than the TFBB-TAB (three/structural unit). The availability of higher number of electrocatalytic sites on the TFBB-TAT offers better water reduction capacity than TFBB-TAB COF. Moreover, the interconnected porous structure enhances the electrolyte diffusion on to the electrode surface resulting in faster electrode kinetics. The interlinked highly conjugated electronic structure of the synthesized COF helps achieve good electronic conductivity. The nitrogen rich TFBB-TAT electrode shows lower charge transfer resistance than TFBB-TAB counterpart. This may be attributed to the better electronic conductivity of former as compared to the latter. The performance of the present TFBB-TAT photocathode was found to be comparable to many previously reported photocathodes for PEC water splitting (**Table T3, ESI**). In the case of TFBB-TAT COF photoanode offers oxygen production capacity 70 µmol cm^{-2} whereas TFBB-TAB COF offers only 15 µmol cm^{-2} after 180 minutes through PEC *via* water splitting reaction (**figure S16, ESI**). [48]

Theoretical and Mechanistic Calculations:

To further prove the exact electron excitation and charge recombination, the band edge position for both the COFs were calculated (**Figure 3f**). The theoretical band gap for TFPB-TAT COF was determined by DFTB calculation to be 2.347 eV with the valence band energy of +0.91913 eV (*vs* NHE) and the conduction band energy of -1.428 eV (*vs* NHE). The absorption spectrum is shown in ESI, **Figure S12**. TFBB-TAT COF absorbs light in the visible range with an absorption threshold of around 540 nm and oneabsorbance maxima at 360 nm with calculated band gap of 2.31 eV which is very close to theoretical band gap (2.347 eV) for slip-AA stacking mode. TFBB-TAB COF shows absorption maxima at 430 nm. In the case of TFBB-TAB shows λ_{max} at ca. 430 nm, as a result, calculated optical band gap of 2.88 eV, which is little higher compare to theoretical band gap (2.29 eV) for slip-AA stacking.[49] This band position shows that the driving force for the proton reduction is enough for the TFFB-TAT COF. However, the transfer of photogenerated hole becomes necessary to reduce the

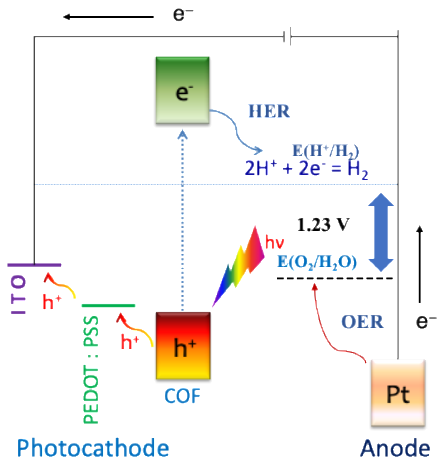

electron-hole pair recombination which helps to improve the effective utilization of photoexcited electrons for proton reduction. Thus, the presence of a proper hole transporting layer will improve the water reduction capacity of the designed photocathode. In present study

Figure 4: Schematic presentation for the possible electron transfer process. This figure represents, PEC water splitting at the COF/ PEDOT:PSS/ITO modified surface as a photocathode for hydrogen evolution reaction (HER) and Pt anode for hydrogen oxygen evolution reaction (OER) under bias free condition. The TFBB-TAT with bandgap energy (Eg) of 2.31 eV is photoexcited under ultraviolet-visible light irradiation.[50]

PEDOT: PSS used as a hole transporting layer for hole transporting from COFs to ITO surface. The valance band maxima of PEDOT: PSS observed at 0.6 eV vs NHE (-5.0 eV vs vacuum) which can easily extract a hole from the valance band of the synthesized COFs. Thus, the efficient charge separation in presence of hole transporting PEDOT: PSS layer offers a promising PEC performance. A schematic of charge transport mechanism of designed photocathode is depicted in Figure 4.

Conclusion:

In conclusion, we present a new triazine based covalent organic framework which shows superior water splitting with respect to the non-triazine counterpart in a photoelectrochemical process. The triazine unit would be play an important role for the light harvesting and electrocatalytic water reduction. The enhanced catalytic activity is due to the large surface area, satisfactory band gap and optimised planar structure leading to better electron charge separation. The photoelectrochemical HER performance of TFBB-TAT COF is comparable or even better in some cases than that of traditional metallic catalysts. The excellent stability and durability of TFBB-TAT COF as a photocathode in presence of light irradiation condition made it a potential candidate for in future efficient photoelectrochemical (PEC) hydrogen evolution

reaction (HER) application. This finding should be of considerable interest to the materials chemistry as well as renewable energy community for next generation organic fuel cells.

Author Contributions

AP designed and synthesized the materials and executed this scheme. MA did the theoretical calculations. All authors discussed the results, commented and wrote the manuscript.

Conflicts of interest

The authors declare there are no conflicts of interest.

Acknowledgements

We also thank Bidhan Chandra Patra and Santimoy Khilari for assistance in experiments. Dr. A. P acknowledge DST-SERB for funding through Inspire faculty and SERB-SRS program. M.A.A acknowledges HPC time through the Materials Chemistry Consortium (EP/P020194).

Notes and references

1 K. Mazloomi and C. Gomes, *Renew. Sust. Energ. Rev.,* 2012, **16**, 3024-3033.
2 J. A. Turner, Science, 2004, **305**, 972-974.
3 M. Cabán-Acevedo, M. L. Stone, J. Schmidt, J. G. Thomas, Q. Ding, H. C. Chang, M. L. Tsai, J. H. He and S. Jin, *Nat. Mater.,* 2015, **14**, 1245-1251.
4 K. Christopher and R. Dimitrios, *Energy Environ. Sci.*, 2012, **5**, 6640-6651.
5 A. Heller, *Acc. Chem. Res.,*1981, **14**, 154-162.
6 M. M. May, H. J. Lewerenz, D. Lackner, F. Dimroth, T. Hannappel, *Nat. Commun.,* 2015, **6**, 8286.
7 N. S. Lewis and D. G. Nocera, *Proc. Natl. Acad. Sci.,* 2006, **103**, 15729.
8 A. Landman, H. Dotan, G. E. Shter, M. Wullenkord, A. Houaijia, A. Maljusch, G. S. Grader and A. Rothschild, *Nat. Mater.,* 2017, **16**, 646-651.
9 S. Y. Tee, K. Y. Win, W. S. Teo, L. D. Koh, S. Liu, C. P. Teng and M. Y. Han, *Adv. Sci.,* 2017, **4**, 1600337.
10 A. Kudo and Y. Miseki, *Chem. Soc. Rev.,* 2009, **38**, 253-278.
11 O. Khaselev and J. A. Turner, *Science*, 1998, 280, 425-427.
12 R. Subbaraman, D. Tripkovic, D. Strmcnik, K. C. Chang, M. Uchimura, A. P. Paulikas, V. Stamenkovic and N. M. Markovic, Science, 2011, **334**, 1256-1260.
13 C. C. L. McCrory, S. Jung, I. M. Ferrer, S. M. Chatman, J. C. Peters and T. F. Jaramillo, *J. Am. Chem. Soc.,* 2015, **137**, 4347-4357.
14 A. B. Laursen, S. Kegnaes, S. Dahl and I. Chorkendorff, *Energy Environ. Sci.,*2012, **5**, 5577-5591.
15 W. Wang, X. Xu, W. Zhou and Z. Shao, *Adv. Sci.,* 2017, **4**, 1600371.
16 J. Li, M. Yan, X. Zhou, Z.Q. Huang, Z. Xia, C. R. Chang, Y. Ma and Y. Qu, *Adv. Funct. Mater.,* 2016, **26**, 6785-6796.
17 A. P. Côté, A. I. Benin, N. W. Ockwig, M. O'Keeffe, A. J. Matzger and O. M. Yaghi, *Science,* 2005, **310**, 1166-1170.
18 F. J. U. Romo, J. R. Hunt, H. Furukawa, C. Klöck, M. O'Keeffe and O. M. Yaghi, *J. Am. Chem. Soc.,* 2009, **131**, 4570-4571.
19 S. Kandambeth, A. Mallick, B. Lukose, M. V. Mane, T. Heine and R. Banerjee, *J. Am. Chem. Soc.,* 2012, **134**, 19524-19527.
20 N. Huang, P. Wang and D. Jiang, *Nat. Rev. Mater.,* 2016, **1**, 16068.
21 D. D. Medina, T. Sick, T. Bein, *Adv. Energy Mater.,* 2017, **7**, 1700387.
22 X. Feng, L. Liu, Y. Honsho, A. Saeki, S. Seki, S. Irle, Y. Dong, A. Nagai and D. Jiang, *Angew. Chem. Int. Ed.,* 2012, **51**, 2618-2622.
23 M. Dogru, M. Handloser, F. Auras, T. Kunz, D. Medina, A. Hartschuh, P. Knochel and T. Bein, *Angew. Chem. Int. Ed.,* 2013, **52**, 2920-2924.
24 J. Xie, S. A. Shevlin, Q. Ruan, S. J. A. Moniz, Y. Liu, X. Liu, Y. Li, C. C. Lau, Z. X. Guo and J. Tang, *Energy Environ. Sci.,* 2018, **11**, 1617-1624.
25 T. Sick, A. G. Hufnage, J. Kampmann, I. Kondofersky, M. Calik, J. M. Rotter, A. Evans, M. Döblinger, S. Herbert, K. Peters, D. Böhm, P. Knochel, D. D. Medina, D. F. Rohlfing and T. Bein, *J. Am. Chem. Soc.,* 2018, 140, 2085-2092.
26 B. C. Patra, S. Khilari, R. N. Manna, S. Mondal, D. Pradhan, A. Pradhan and A. Bhaumik, *ACS Catal.,* 2017, **7**, 6120–6127.
27 S. Bhunia, S. K. Das, R. Jana, S. C. Peter, S. Bhattacharya, M. Addicoat, A. Bhaumik and A. Pradhan, *ACS Appl. Mater. Interfaces,* 2017, **9**, 23843–23851.
28 A. Pradhan and R. N. Manna, *ACS Appl. Polym. Mater.,* 2021, **3**, 1376–1384.
29 L. Stegbauer, K. Schwinghammer and B. V. Lotsch, *Chem. Sci.,* 2014, **5**, 2789-2793.
30 V. S. Vyas, F. Haase, L. Stegbauer, G. Savasci, F. Podjaski, C. Ochsenfeld and B. V. Lotsch, *Nat. Commun.,* 2015, **6**, 8508.
31 X. Jiang, P. Wanga and J. Zhao, *J. Mater. Chem. A,* 2015, **3**, 7750-7758.
32 M. M. May, H. J. Lewerenz, D. Lackner, F. Dimroth and T. Hannappel, *Nat. Commun.,* 2015, **6**, 8286.
33 L. Yao, A. R. Camargo, M. Xia, D. Mücke, R. Guntermann, Y. Liu, L. Grunenberg, A. J.Solano, S. T. Emmerling, V. Duppel, K. Sivula, T. Bein, H. Qi, U. Kaiser, M. Grätzel, and B. V. Lotsch, *J. Am. Chem. Soc.* 2022, **144**, 10291-10300.
34 B. Aradi, B. Hourahine and Th. Frauenheim, *J. Phys. Chem. A,* 2007, **111**, 5678–5684.
35 Q. Sun, B. Aguila, J. Perman, L. D. Earl, C. W. Abney, Y. C. Cheng, H. Wei, N. Nguyen, L. Wojtas and S. Q. Ma, *J. Am. Chem. Soc.,* 2017, **139**, 2786-2793.
36 Q. Wang, Y. S. Gao, J. Z. Luo, Z. Y. Zhong, A. Borgna, Z. H. Guo and D. O'Hare, *RSC Adv.*, 2013, **3**, 3414–3420.
37 S. K. Das, S. Mishra, K. Manna, U. Kayal, S. Mahapatra, K. D. Saha, S. Dalapati, G. P. Das, A. A. Mostafa, A. Bhaumik, *Chem. Commun.,* 2018, **54**, 11475-11478.
38 I. Hisaki, Y. Suzuki, E. Gomez, Q. Ji, N. Tohnai, T. Nakamura, and A. Douhal, *J. Am. Chem. Soc.,* 2019, **141**, 2111-2121.
39 L. Grunenberg, G. Savasci, M. W. Terban, V. Duppel, I. Moudrakovski, M. Etter, R. E. Dinnebier, C. Ochsenfeld, and B. V. Lotsch, *J. Am. Chem. Soc.,* 2021, **143**, 3430-3438.
40 C.G. Morales-Guio, S. D. Tilley, H. Vrubel, M. Grätzel and X. Hu, *Nat. Commun.,* 2014, **5**, 3059.
41 Y. Zheng, Y. Jiao, Y. Zhu, L. H. Li, Y. Han, Y. Chen, A. Du, M. Jaroniec, S. Z. Qiao, *Nat. Commun.,* 2014, **5**, 3783.
42 C. J. Chen, P. T. Chen, M. Basu, K. C. Yang, Y. R. Lu, C. L. Dong, C. G. Ma, C. C. Shen, S. F. Hu and R. S. Liu, *J. Mater. Chem. A*, 2015, **3**, 23466-23476.
43 C. A. Downes and S. C. Marinescu, *J. Am. Chem. Soc.,* 2015, **137**, 13740-13743.
44 P. Meng, M. Wang, Y. Yang, S. Zhang and L. Sun, *J. Mater. Chem. A*, 2015, **3**, 18852-18859.
45 Z. S. Wu, L. Chen, J. Liu, K. Parvez, H. Liang, J. Shu, H. Sachdev, R. Graf, X. Feng and K. Müllen, *Adv. Mater.,* 2014, **26**, 1450-1455.
46 Z. Chen, H. N. Dinh and E. Miller, Photoelectrochemical Water Splitting: Standards, Experimental Methods, and Protocols, Springer, New York, 2013.
47 S. Bhunia, K. Bhunia, B. C. Patra, S. K. Das, D. Pradhan, A. Bhaumik, A. Pradhan, S. Bhattacharya. *ACS Appl. Mater. Interfaces,* 2019, **11**, 1520-1528.

Formatted: English (United Kingdom)

48 M. A. Khan , P. Varadhan, V. Ramalingam, H. C. Fu, H. Idriss, and J. H. He, *ACS Energy Lett.* 2019, **4**, 2712−2718.
49 T. Sick, A. G. Hufnagel, J. Kampmann, I. Kondofersky, M. Calik, J. M. Rotter, A. Evans, M. Döblinger, S. Herbert, K. Peters, D. Böhm, P. Knochel, D. D. Medina, D. F. Rohlfing and T. Bein, *J. Am. Chem. Soc.*,2018, **140**, 2085-2092.
50 A. Fujishima and K. Honda, *Nature* 1972, **238**, 37-38.

TOC